A Simple Pendulum Design and Calibration

David Petrushenko
Virginia Tech
Dept. of Mechanical Engineering
Blacksburg, Virginia
petrusd26@vt.edu

Joshua R. Tempelman
Dept. of Mechanical Engineering
Michigan State University
East Lansing, MI
tempelm2@msu.edu

Audun D. Myers
Dept. of Mechanical Engineering
Michigan State University
East Lansing, MI
myersau3@msu.edu

Firas A. Khasawneh
Dept. of Mechanical Engineering
Michigan State University
East Lansing, MI
khasawn3@egr.msu.edu

February 27, 2020

Referencing this work

Please reference the work and CAD presented using the following papers: "Uncertainty Propagation of System Parameters to the Dynamic Response: An Application to a Benchtop Pendulum" [3] and (soon to be published) "Dynamic State Analysis of a Driven Magnetic Pendulum Using Complex Networks."

Contents

1 Introduction

This document provides a description of the design, manufacturing, and assembly of a simple pendulum and calibration apparatus. The simple pendulum assembly discussed in this document is designed to be used in a laboratory setting. With any experimental work, it is critical to have experimental procedures and designs well documented. It is the goal of this document to provide the reader with an adequate understanding of the design considerations and methodology associated with the simple pendulum design and calibration set up.

A description of the assembly of the pendulum and coupling between encoder and pendulum is given in section 2. A brief description of the encoder calibration process is provided in section 3. Section 3.2 expands on the design process for the accompanying calibration assembly, and detailed descriptions of the design are given in 3.2.1. These sections provide details on the considerations of the functionality and manufacturability of the calibration assembly. Since 3D printing was used to manufacture a majority of components of the pendulum and calibration assemblies, section 3.3.1 is included to provide insight on good printing practices. Technical details pertaining to the height of the calibration bars and the geometric relationships and uncertainties of the calibration process are given in sections 3.4 and 3.5 respectively. We have also added new adaptations to the simple pendulum for incorporating a repulsive magnetic force. The design, model, and experimental parameters for this adaptation are provided in Section 4.

2 Pendulum Assembly

An experimental assembly was designed to securely mount the pendulum pivot while still offering minimum damping. Additionally, the pendulum must be connected to an analog encoder in order to record the angular position of the arm during operation. Hence, a mechanical coupling must be configured between the pendulum pivot and the encoder which is rigid and provides low friction. It is imperative that the base remains rigid and stationary while the pendulum is moving in order to prevent distortions to measurements. Any deformation in the base structure during an experiment may create noisy or corrupt data. Any distortion or movement of the single pendulum base or mechanical coupling would effect the behavior of the system, so the design of the pendulum housing must respect these constraints.

2.1 Base Structure

The pendulum base is a one-piece structure which has been manufactured with 3-D printing. The plastic print provides structural stability using A-frames and thick support ribs whose cross section is 0.5" $\times$ 0.5". Additionally, the corners of these support ribs feature a large radius which minimized stress concentrations in the structure. With the reinforcement provided to the base, the forces induced by the pendulum will not be large enough to generate any notable deformation in the base structure. Additionally, the base structure features through holes on the bottom-surface which are sized to fit 1/4-20 machine screws and are spaced to be compatible with an optical table as shown in Figure 14. A total of six screws are used to secure the base structure to the optical table. For considerations of the thickness of the bottom surface, it is recommended to use screws which are at least 1 1/4 inches. A cylindrical section near the top of the base is left hollow to serve as the housing for the coupling between the pendu-

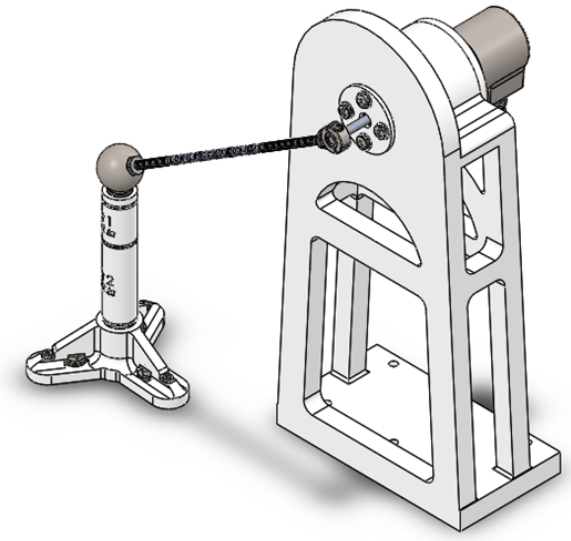

Figure 1: Pendulum assembly

lum and encoder, and four small holes surround the
perimeter of this feature on both the front and back side of the base structure to allow for flanges to connect a bearing in the front and the encoder in the back. For more information on this feature refer to section 2.2.

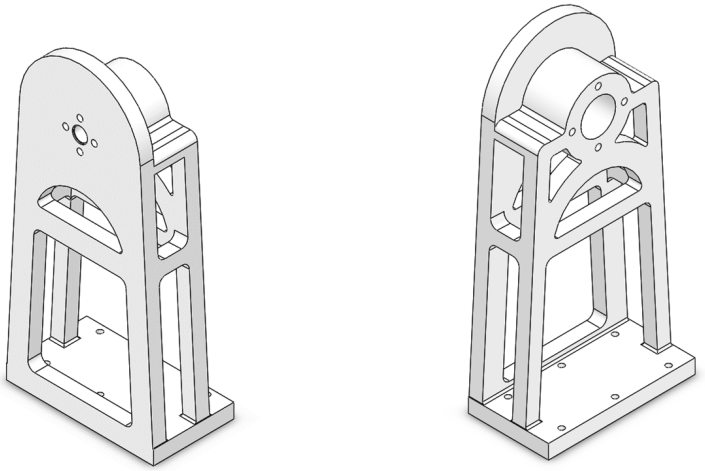

(a) Front view (b) Back view

Figure 2: Base structure for pendulum assembly

2.2 Pendulum to encoder coupling

The mechanical coupling between the pendulum and the encoder, as shown in Figure 3, provides a means to correspond the angle of the encoder to the angle of the pendulum. To do this, the 10-32 threaded pendulum shaft is secured to a clamp collar which features matching female threading. At the opposite end of the pendulum shaft sits a spherical steel mass which also threads onto the pendulum shaft. The clamp collar uses machine screws to secure a 0.1875 inch-diameter precision ground connecting rod, and this rod connects to a clamping precision flexible shaft coupling. A flexible shaft coupling is commonly used for light duty encoder and stepper drive applications. It is advantageous to use such a product because it does not need lubrication, provides zero backlash, and is more forgiving of misalignment. The shaft coupling must also connect the encoder shaft to the pendulum shaft which have dissimilar diameters.
The features of this particular coupling feature a parallel misalignment capability of 0.2mm, an angular misalignment capability of 2°, and an axial misalignment capability of 0.12mm. To support the connecting rod, a flanged ball bearing is used at the front of the pedestal. The bearing is located midway between the clamp collar and the flexible coupling, and it is secured in place with a flange which connects to the pedestal. It's lubricated and shielded, and the dynamic and static load ratings of 290 lbs and 100 lbs respectively far exceed the forces which the bearing will endure from the pendulum.

To secure the flange to the Pedestal, four 8-32 × 0.5 inch pan head cap screws are used. 8-32 E-Z LOK threaded inserts are positioned in the four hole pattern featured on the Pedestal. The pan-head cap screws secure the bearing flange in place, and plastic washers are utilized to protect the flange from the screws. The inner-bore on the flange is used to seat the bearing. On the back side of the assembly, the rotary encoder is held in position with a similar flange. The rotary encoder flange utilizes the same method as the bearing flange to attach to the base. The encoder flange is much larger, however, and the
four additional holes are featured on this part which must match the configuration of the MCD-AVP02-0412-CRW flange which comes attached to the rotary encoder. Four M3 socket head cap screws can be used to attach the encoder to the encoder flange, and like the bearing flange, four 8-32 x 0.5 inch pan head cap screws with matching 8-32 E-Z LOK threaded inserts and plastic washers are used to attach the encoder flange to the base structure. Figure 3 provides a visual of the coupling assembly without the base structure.

For reference on where this coupling is found on the assembly, see Figure 1. The encoder features a small shaft, and the angle of this shaft controls the output of the encoder. The shaft of the encoder is secured to the clamping precision flexible shaft coupling by adjusting the clamping screw of the coupling, thus connecting the input shaft of the encoder to the pendulum. With this connection complete, the assembly is fully constructed. Note that all manufactured parts in this assembly were produced using 3D printing.

3 Encoder Calibration

To calibrate the encoder, a multipoint measurement procedure was performed to prepare for collecting data. The simplistic approach taken to calibrate the encoder utilized assembly measurements along with geometric relations to develop a linear relationship between the encoder's angular position and voltage output. The subsequent sections provide a detailed description of the calibration process beginning with the design of the pendulum calibration setup and concluding with the relationship established between the voltage and angle of the encoder. We begin by describing the details of the design iterations and successive improvements made in each iteration.

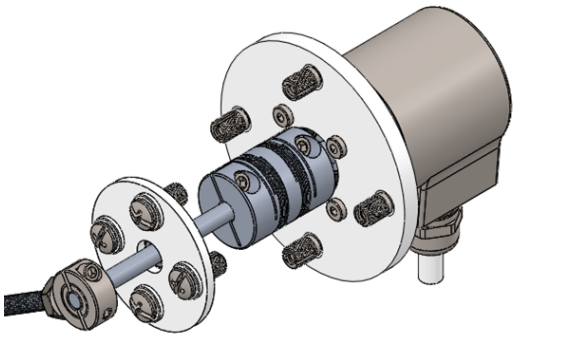

(a) View 1

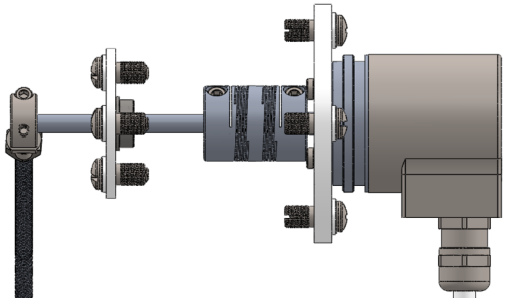

(b) Side view

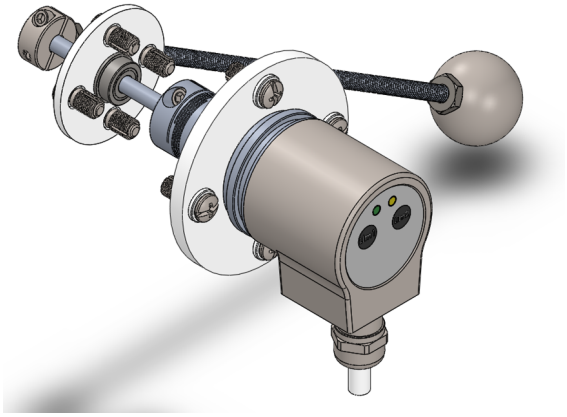

(c) View 2

Figure 3: Mechanical coupling assembly

3.1 Calibration methodology

Knowing that the encoder has a linear range of 10V and a minimum swing angle of 22.5 degrees , after fastening the pendulum to the lab table, the pendulum arm was set on the calibration setup on bar 2, which made an angle slightly larger than 30 degrees (the linear pendulum range). This was done with intent of reducing the nonlinear behavior of the voltage of the encoder once it approaches its extremes on the output voltage range. The pendulum arm was placed on selected vertically measured heights At each elevation, a time series was recorded and further analyzed along with measured values of the height and the pendulum arm providing an angular value. The calculated angular values were then plotted with the corresponding time series voltage values onto as Cartesian coordinates. A linear least-squares fit curve was fitted to the data providing a linear relation between the voltage output of the encoder and the angle the pendulum arm made with the negative vertical axis, positive angles taken to be counterclockwise and negative angles clockwise [to follow typical mechanical engineering right hand rule notation]. To gather a more precise calibration curve, it is important to note that the heights at which the arm is rested upon must be noted to the highest level of precision to reduce the error associated with determining the uncertainty of the collected measurements. For a larger set of data, angular output values may be gathered on the positive and negative side of the pendulum setup.

Using relationships which are defined in section 3.5 which relate the calibration assembly surface height to an angle, the system may be calibrated by associating the voltage

outputs with the numerous calibration height options. The voltage may be set to zero at an angle of zero which is found when the pendulum free-hanging in a completely vertical orientation. With the encoder respecting this $\theta = 0$ condition, the voltage recordings found at the numerous calibration configurations will result in a linear relationship between the output voltage of the encoder and the angle of the pendulum.

3.2 The Calibration Setup Design Concept

The intent of the calibration setup was to provide a simple design able to be replicated in minimal time and with minimal manufacturing operations.

Design Criteria: Considering the application of the design, it was desirable to make an easily adjustable portable structure. Stability of the structure is important since the pendulum requires a number of angular measurements which require rotation at large angles. Producing a tall structure with good stability is critical for reducing the errors associated with deflection of the setup. As typical for most designs, an effort was made to decrease the number of parts required to be manufactured and purchased while capturing the design intent considering the available resources. Such a design is best suited to be produced on a rapid prototyping machine since it requires one instance of production and one of assembly.

Rapid prototyping machines have become common and are accessible with limited knowledge of the manufacturing process allowing for replication of a design with relative ease. The concept presented in Figure 4 may be divided into three primary components; a cap for resting the pendulum arm, posts for controlling the height, and a base to stabilize and support the structure. Successive concept iterations of the individual parts were considered in an effort to improve and achieve the most effective design. The improvements implemented between iterations are presented and discussed briefly in the succeeding sections.

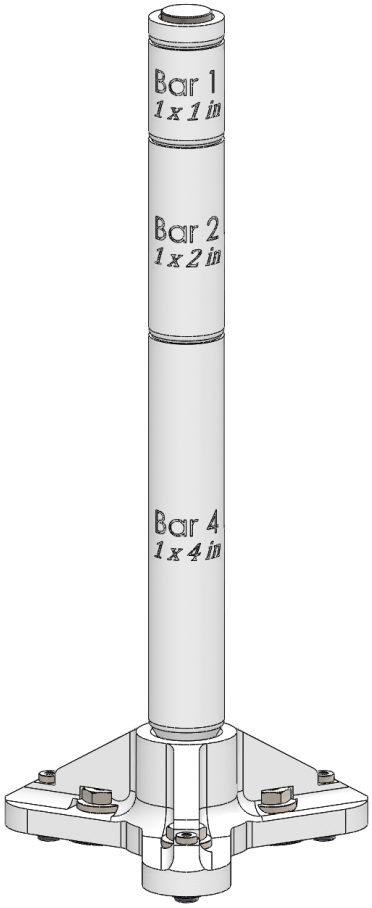

Figure 4: Calibration Assembly

3.2.1 Base Design

In the present discussion, it is assumed that the pendulum is mounted to a table having a flat surface. The primary purpose of the base is to position the post of the calibration assembly across the pendulum pedestal to ensure for proper calibration. Three different contact points were used to locate the base on the table. The mating geometry between the base and the post will be discussed in section 3.3. The segment connecting the base mating geometry to the rests was designed with the intention to minimize even the slightest deformations produced by the combined weight of the pendulum arm and the calibration posts. With the triangular vertical rib, forces acting on the base are immediately transferred to the centers of the three rest pads. Similarly, the horizontal brim acts to stiffen and prevent the vertical ribs from deviating from their respective positions. Together, these two features work to provide a rigid method of weight transfer to the three contact points without experiencing significant deflection. Considering the volume occupied by the part and the density of the plastic print material, it was determined that the base would be very light. Consequently, resting the pendulum arm on the assembly will induce a force acting to tip the structure; especially in the taller configurations of the calibration setup.

To overcome the potential of having the base of the structure tip or levitate under this condition, magnets were added to the underside of the base. Working on a metallic optical table top, the magnet attracts the base effectively giving it more stability to resist small forces acting to tip the structure. The size of the magnet was chosen to provide an approximate additional five pounds of force. Respecting the symmetry of

the base, the magnets were positioned near the resting pads. Three screws were added to secure the magnets to the base of the structure as shown in the section view of Figure 5. The base may be printed on a flat surface reducing the use of support material and the overall time of the print.

Rotating swivel pads were added as part of the base as shown in the section view of Figure 5. These parts allow the replacement of the swiveling pads in the event that they wear significantly or if a harder material such as steel is desired as opposed to plastic. Appropriate sized screws were added to secure the parts in place and prevent them from falling out. The configuration chosen for this instance was with delrin feet to avoid scratching the optical table surface. A variety of pad materials are available from the manufacturer of this product.

The center bore in the base as shown in Figure 5 is sufficiently large enough to fit a 1/4-20 stud from mating parts which can be secured with an appropriately sized nut without protruding past the bottom surface of the base.

The three base magnets were positioned with no material interfering with their attraction to the metallic surface. Washer/nut mechanism may be used to adjust the force that the magnets add to the base by moving the magnets closer or further from the table. This was mainly done with the intent of using the base to support items that will have some sort of force acting to tip the assembly over. Also, if the calibration assembly begins to get very tall, the magnets may be adjusted to accommodate the force acting through the bars as a lever on the top surface of the cap. Screws were used in their most effective orientation; pulling on the threads. The load is transferred through them to the vertical ribs which then transfer the load to the pads.

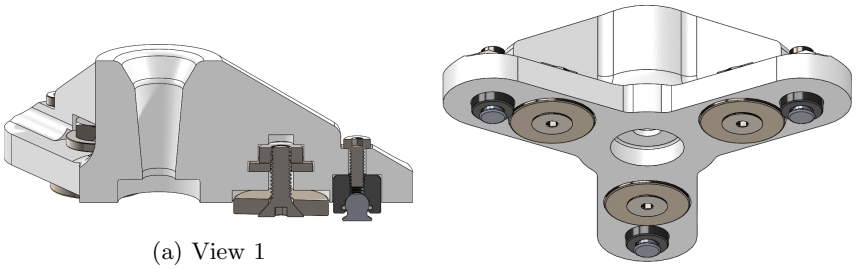

(a) View 1

(b) View 2

Figure 5: Base Design Iteration 3

3.3 Post Design

Some things to consider:

- Providing an appropriate mating geometry to allow for quick assembly and disassembly.
- The mating profile was kept the same for all of the pieces in an effort to "standardize" the parts to mate with each other in the various configurations.
- Height of the individual bars may be adjusted to accommodate the various heights of the pendulum and the number of bars may also be increased as needed.
- Post markings are there to describe the total height of the individual post and may be referenced to the design table in the model.
- The most efficient way of making the larges amount of configurations of heights is to utilize the binary system - 1,2,4,8,... The number of posts may be increased to accommodate various heights of the pendulum by continuing the design table in the model as well as the binary table in this document.

3.3.1 Considerations of the Print

- Depending on the printer to be used, in general is is wise to keep at least 1 surface of the part flat. 3D printers with support material are not effected by this as much, however, this is good design practice to minimize the use of support material which further reduces the cost of the part. The base was designed with minimal abnormalities to the base surface. In the vertical direction, it is wise to keep drafts to a minimum in the outside direction. The base design incorporates this guideline since the overall cross - sectional area of the base continues to decrease in size as the height increases.
- The base design was constructed in such a manner as to reduce the amount of support material required for the print. If oriented with the pads down, the print should use very little support material. All moving up from the base, there is no negative draft in the design - only positive or none at all. This will allow for a cheaper print overall with most of the material being the actual object material.
- The printing of the bars should be done vertical to reduce the distortion of the bars. Our initial print was done horizontal to reduce print time but it resulted in bars having a "banana" effect (bow) and did not have good conical mounting surfaces
- Reducing volume (and thus weight) is a key component in 3D printing since those are typically the deciding factors of the print. Each part was designed to keep a low profile and have only the features required to not "compromise" the desired outcome.
- Each mating feature used on the design requires some clearance for assembly. If the parts are printed with nominal dimensions, depending on the quality of the print, the parts may not fit together very well. Therefore, it is important to use proper tolerances as recommended by the manufacturer mating features/surfaces.

3.3.2 Base design highlights

- The base requires 3 contact points (# of points to locate on plane). The idea of only needing 3 points was incorporated in the design by having only three of every item. The bore found on the bottom of the base is intentionally there to provide the ability to rigidly connect an item to the base if it is required. A stud may be used in the male part, and a nut may be used to fasten the part without being in the way. The thread size that will fit through the hole is 1/4" with the same respective nut size to connect it. The height profile was kept to a minimum to allow the measurement of small angles from the vertical position of the pendulum. Depending on the height of the pendulum, this may or may not be a problem. It is nice to keep the bottom surface flat to
- Fairlane BBU - 100 - DC Swivots with Delrin cone used to avoid scratching optical table surface. Also, the configuration of the model may be changed to print the spherical pads for a more cost - friendly approach.
- Pads are removable - attached by #4-40 screws. May be replaced with similar profile feet that are potentially found cheaper elsewhere. The model may also be modified to accommodate this change if required. Other suggested feet provided by the manufacturer are stainless steel, diamond surface, or urethane. These feet are designed for industrial use and can withstand considerable use before wearing. This was the primary thought behind using manufactured feet was to resist potential wear of the manufactured base.
- Ribs provide rigidity for the design by removing almost all of the deflection experienced by the setup from weight of pendulum and the assembly itself. The ribs were filleted to provide a smooth transition between surfaces and for aesthetics.
- Magnets are implemented for additional stability to the assembly especially when it begins to get quite high. These items are not required and may be removed upon consideration. However, if the base is used for other applications, it may be useful to have the additional support. The overall density will be relatively low if manufactured by 3D printing meaning a lower total mass. Magnets will help keep the base from tilting and causing a false measured value. Magnets were placed as close to the feet of the base as possible to remove the deformation they may potentially induce on the design. Using magnets limits the surface on which they may be used to metallic. A small screw was used to prevent

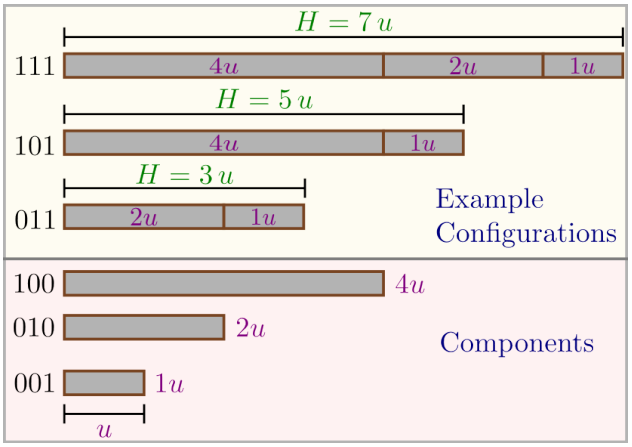

Figure 6: An example showing the component lengths for 3 pieces for the calibration assembly and some example configurations. Three examples are shown for $H = 3\,u$, $5\,u$, and $7\,u$. Each example uses a different stacking of the components. The binary representation for each component and assembly is shown on the left side of the parts.

the magnets from falling out of the pockets. A small pin may also be used since the magnet will instantly be attracted to it preventing it from falling out. Magnets were chosen to give a sufficient amount of force without providing more force than required and deforming the base. Magnets were made adjustable by the screws to allow for adjustment of the force of them. For various uses, the base may be used with a mechanical solid connection requiring more force. You will need to loosen the screws for all of the magnets and the attraction becomes greater.

- The configuration of the mating surfaces at the base was chosen with the thought of making detaching very quick and the results of re-stacking repeatable. The double conical surface works to minimize distance of the mating feature while respecting stability. The smaller conical surface acts to stabilize the stacking of the bars that will be placed on top of the base. The idea of using a cone results from the inability of 3D printing to provide the best results in terms of repeat-ability and surface quality. Ideally, a process which produces a repeatable cylindrical surface would yield the most stable structure. However, the smaller angle will help align the different asymmetrical parts. The smaller the angle the better because if you take the surface normal vector and split up into components, you will find that the component of greatest magnitude is perpendicular to the central axis of the base. This is the component most important in stabilizing the vertical bars from moving around with respect to the base. In theory, if the print used on the manufacturing of these bars is fine enough, the small angle may be made even smaller. The large angle acts as a "seat" for the vertical bars. The surface normal vector of the large conical angle results in the same components parallel and perpendicular the axis of the part. This will further help stabilize the vertical bars from moving with respect to the axis and terminate their downward movement at a particular height. Fillet were added in the female mating part prevent chipping of the corners allow any imperfections in the male mating sharp corner to not interfere with the mating.

3.4 Choice of heights for the calibration assembly

With the requirement of quickly adjusting the height of the calibration tower, one question is how to design the lengths of its different parts. A guiding constraint is having the ability to cover the maximum range of heights using the minimum number of components. Assume that the maximum height $H = N\,u$ is some integer multiple N of a height unit u. This formulates the problem as that of breaking the integer N into the smallest number of components that add up to N, and that in addition the components can be combined to cover the range from 1 to N.

For example, assume that we would like to cover a range of $H = 7\,u$, i.e., $N = 7$. One straightforward

choice is to make 7 pieces, each of length u; however, this does not satisfy the requirement of minimizing the number of pieces. An alternative approach is shown in Figure 6, where we visualize the calibration height as the stacking of parts whose presence is indicated by 0 for not present, or 1 for present. This leads us to viewing this problem as that of a binary representation of the height of the calibration assembly. Specifically, for the the example of $H = 7\,u$, we can get $N = 7$ according to

$$7 = 1 \times 2^0 + 1 \times 2^1 + 1 \times 2^2. \tag{1}$$

This means that we need to stack 3 pieces of lengths 1, 2, and 4 to get the desired height of $7\,u$. Figure 6 shows two other examples for $H = 3\,u$ and $H = 5\,u$. In general, if we are using a number of height pieces n, then we can cover the range $H \in [0, (2^n - 1)\,u]$ using parts of lengths $\{2^0, 2^1, 2^2, \ldots, 2^{n-1}\}$. Therefore, the height of the calibration assembly can be designed and extended in a systematic way if more calibration points are needed. For our design, we chose $u = 1$ inch and printed 3 pieces so that the calibration tower can be raised to 7 inches on top of its base height, see Figure 4.

3.5 Geometric relationships and uncertainties

Simple geometric relations are applied when calibrating the encoder. For a visual representation of the variables in this passage, refer to Figure 7. If we take the length of the rod arm spanning from the center of the pivot to the center of the end mass to be $l_{arm} \pm \delta l_{arm}$ and the vertical distance between the center of the end mass to the center of the pivot to be $\Delta h \pm \Delta\delta h$, then the resulting angle of the pendulum arm can be found with:

$$\cos\theta = \frac{\Delta h \pm \delta\Delta h}{l_{arm} \pm \delta l_{arm}} \tag{2}$$

The uncertainties of l_{arm} and Δh of equation 2 must be considered. Δh is not measured directly, rather it is

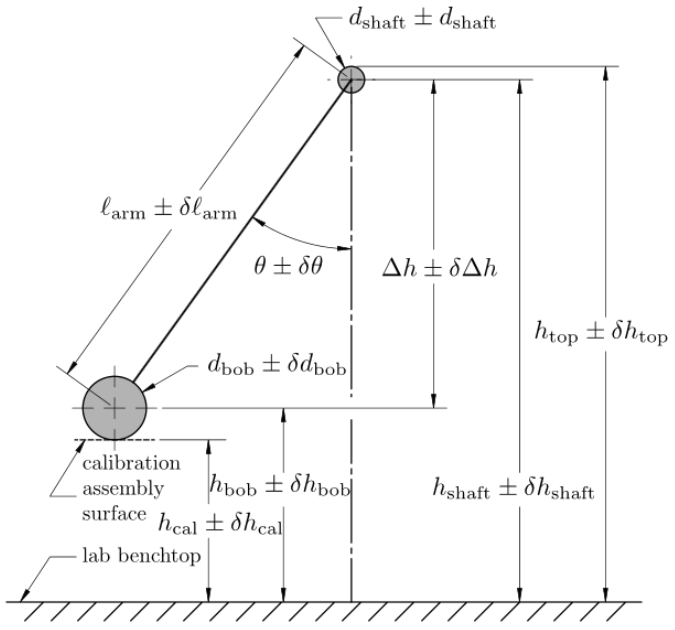

Figure 7: Simple pendulum calibration layout.

found with several different measurements all with their own independent uncertainties. h_{cal} and h_{top} is the height of the calibration assembly surface and top of the precision rod shaft respectively. Additionally, d_{bob} and d_{shaft} represent the diameter of the rod end mass and precision rod respectively. The value of interest

in equation 2 can now be found by relating the measurements with $\Delta h = h_{top} - h_{cal} - \frac{1}{2}(d_{bob} + d_{shaft})$. Accounting for uncertainties in measurements, this is more properly noted as:

$$\Delta h \pm \delta\Delta h = (h_{top} \pm \delta h_{top}) - (h_{cal} \pm \delta h_{cal}) - \frac{1}{2}((d_{bob} \pm \delta d_{bob}) + (d_{shaft} \pm \delta d_{shaft})) \tag{3}$$

Since addition and subtraction is used between the measured variables, and because the measurement of the variables is independent, it is appropriate to sum the independent uncertainties in quadrature to find the uncertainty of Δh.

$$\delta\Delta h = \sqrt{(\delta h_{top})^2 + (\delta h_{cal})^2 + \left(\frac{1}{2}\delta d_{bob}\right)^2 + \left(\frac{1}{2}\delta d_{shaft}\right)^2} \tag{4}$$

For products and quotients of terms with independent uncertainties, the resulting uncertainty is found by summing the percent uncertainty, $|\frac{\delta q}{q}|$, in quadrature. Likewise, the uncertainty which propagates through a mathematical operator such as arccos, the uncertainty of the term is equal to the derivative of the operator multiplied by the uncertainty of the term which is operated on, or $\delta q = |\frac{dq}{dx}|\delta x$. By re-ordering equation 2 so that $\theta \pm \delta\theta = \arccos\left(\frac{\Delta h \pm \delta\Delta h}{l_{arm} \pm \delta l_{arm}}\right)$, maintaining the relationships of equations 3 and 4, and noting $\frac{d}{dx}\arccos(x) = \frac{1}{-\sqrt{1-x^2}}$, the value and uncertainty of θ is given with equation 5

$$\theta \pm \delta\theta = \arccos\left(\frac{\Delta h}{l_{arm}}\right)\left(1 \pm \frac{\sqrt{\left(\frac{\delta\Delta h}{\Delta h}\right)^2 + \left(\frac{\delta l_{arm}}{l_{arm}}\right)^2}}{\sqrt{1 - \left(\frac{\Delta h}{l_{arm}}\right)^2}}\right) \tag{5}$$

4 The Magnetic Pendulum Adaptation

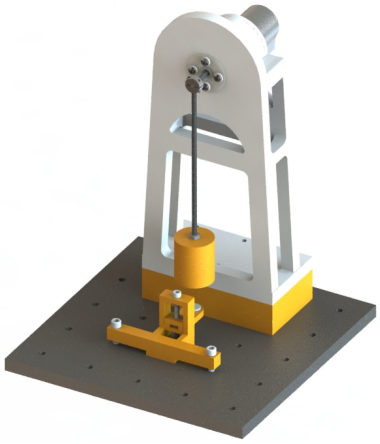

Figure 8: Adaptations to make magnetic pendulum.

In this section we will introduce a simple adaptation to the previously described pendulum to introduce a repulsive magnetic force. The driven magnetic pendulum is a well known system to exhibit chaos [4, 5, 2]. This makes adding this adaptation a simple way to introduce much more complicated dynamics. In Fig. 8, a rendering of the adaptations are shown. In this section we will derive a simplified equation of motion using Lagrange's Equation. The design, manufacturing, and equipment used for the experiment are also briefly mentioned. Additionally, we will introduce our methods for estimating and measuring the constants in the equation of motion.

4.1 Model

To begin a numerical investigation into the base-excited single magnetic pendulum, we need to first develop a simplified model of the physical system (see Fig. 9). The first simplification done was reducing all the

connected components that make the oscillating mass of pendulum to a single mass M with an effective inertia about the I_o and distance to the center of mass r_{cm}. The second simplification was to reduce the magnetic force model to a dipole model with $m_1 = m_2 = m$ as the dipole moment magnitudes. To develop the equation of motion, we use Lagrange's Equation (Eq. (14)), which is then used to simulate the system. To use Eq. (14), the potential energy V, kinetic energy T, and non-conservative moments R are needed. In this analysis the damping moments and the moments generated from the magnetic interaction are treated as non-conservative. The potential and kinetic energy are defined as

$$\begin{aligned} T &= \frac{1}{2}M|\vec{v}_{cm}|^2 + \frac{1}{2}I_{cm}\dot{\theta}^2, \\ V &= -Mgr_{cm}\cos(\theta), \end{aligned} \tag{6}$$

where $\vec{v}_c m$ is the velocity at the center of mass, which is calculated as

$$\vec{v}_{cm} = r_{cm}\dot{\theta}\left[\cos(\theta)\hat{\epsilon}_x + \sin(\theta)\hat{\epsilon}_y\right] + A\cos(\omega t)\hat{\epsilon}_x. \tag{7}$$

In Eq. (7), $A\cos(\omega t)$ is introduced from the base excitation $b(t) = A\cos(\omega t)$ in the x direction with A as the amplitude and ω as the frequency and $\hat{\epsilon}_x$ and $\hat{\epsilon}_y$ are the unit vectors in the x and y directions, respectively.

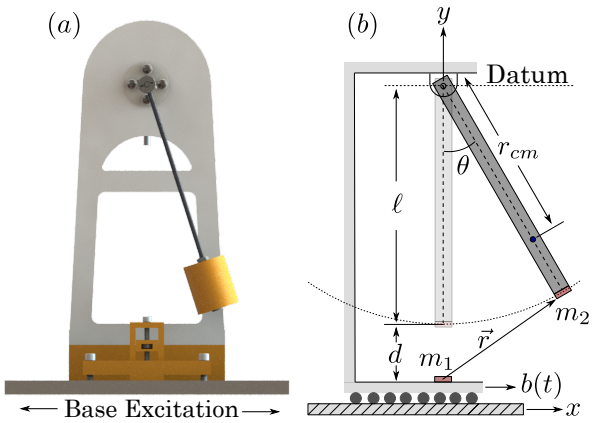

Figure 9: Rendering of experimental setup in comparison to reduced model, where $b(t) = A\sin(\omega t)$ is the base excitation with frequency ω and amplitude A, r_{cm} is the effective center of mass of the pendulum, d is the minimum distance between magnets $m_1 = m_2 = m$ (modeled as dipoles), and ℓ is the length of the pendulum.

The non-conservative moments are caused by the natural energy lose from damping. For our analysis, we consider three possible mechanisms of energy dissipation: Coulomb damping τ_c, viscous damping τ_v, and quadratic damping τ_q. We chose to use all three mechanisms of damping due to previous work on parameter estimation for a similar pendulum [3]. These three moments are defined as

$$\begin{aligned} \tau_c &= \mu_c \text{sgn}(\dot{\theta}), \\ \tau_v &= \mu_v\dot{\theta}, \\ \tau_q &= \mu_q\dot{\theta}^2\text{sgn}(\dot{\theta}), \end{aligned} \tag{8}$$

where μ_c, μ_v, and μ_q are the coefficient for Coulomb, viscous, and quadratic damping, respectively.

We will now introduce the derivation of the torque induced from the magnetic interaction τ_m. To begin, consider two, in-plane magnets as shown on the left side of Fig. 10, where the red side of the magnet represents its north-pole. From this representation, the magnetic force acting on each magnetic is calculated as

$$\begin{aligned} F_r &= \frac{3\mu_o m^2}{4\pi r^4}\left[2c(\phi-\alpha)c(\phi-\beta) - s(\phi-\alpha)s(\phi-\beta)\right], \\ F_\phi &= \frac{3\mu_o m^2}{4\pi r^4}\left[s(2\phi-\alpha-\beta)\right], \end{aligned} \tag{9}$$

where m_1 and m_2 are the magnetic moments, μ_o is the magnetic permeability of free space, and $c(*) = \sin(*)$ and $s(*) = \sin(*)$. Equation (9) assumes that the cylindrical magnets used in the experiment can be approximated as a dipole. This assumption will be shown as satisfactory in Fig. 12 of Section 4.3. These

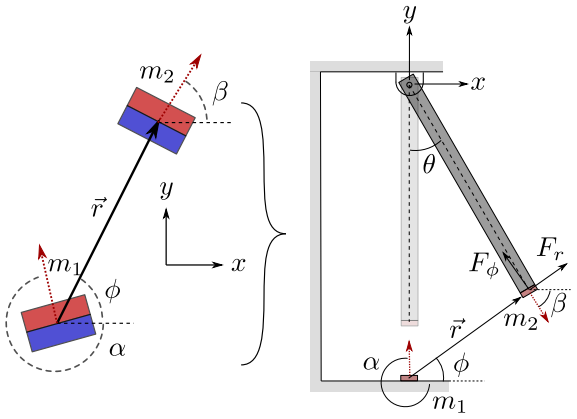

Figure 10: A comparison between a generic, in-plane magnetic model in global coordinates and the equivalent magnetic forces in the pendulum model F_r and F_ϕ (see Eq. (9)).

magnetic forces are then adapted to the physical pendulum as shown on the right side of Fig. 10, with $\alpha = \pi/2$ and $\beta = \pi/2 - \theta$. Additionally, ϕ and r are calculated from θ, d, and ℓ from Fig. 9 as

$$\phi = \frac{\pi}{2} - \arcsin\left(\frac{\ell}{r}\sin(\theta)\right) \tag{10}$$

and

$$r = \sqrt{[\ell\sin(\theta)]^2 + [d + \ell(1 - \cos(\theta))]^2}. \tag{11}$$

The moment induced from the magnetic interaction is then

$$\tau_m = \ell F_r \cos(\phi - \theta) - \ell F_\phi \sin(\phi - \theta). \tag{12}$$

Using τ_m from Eq. (12) and the non-conservative torques from Eq. (8), R is defined as

$$R = \tau_c + \tau_v + \tau_q + \tau_m. \tag{13}$$

Finally, the equation of motion for the base-excited magnetic single pendulum is found by solving Lagrange's equation as

$$\frac{\partial}{\partial t}\left(\frac{\partial L}{\partial \dot{\theta}}\right) - \frac{\partial L}{\partial \theta} + R = 0, \tag{14}$$

where $L = T - V$. Equation (14) was symbolically manipulated to be in a state space format using Python's *Sympy* package. Then, the system was simulated at a frequency of $f_s = 60$ Hz using Python's *odeint* function from the *Scipy* library.

4.2 Equipment and Design of Experiment

The setup of the experiment was manufactured by modifying a previously studied single pendulum [3]. To increase the non-linearity, in-plane magnets on the base as well as at the end of the pendulum were added. To assume a permeability of free space μ_0, any ferromagnetic material within the vicinity was removed, which made the use of 3D printed components critical. In Fig. 11 an overview of the additional components from the original pendulum are shown. Specifically, in Fig. 11 (a) and (b), the exploded views of the linear stage for controlling the distance d and the end mass of the pendulum are shown. The magnets used are two, approximately identical, rare-earth (neodymium) N52 permanent magnets with a radius and length of 1/4" (6.35 mm).

Table 1 provides a list of the item, description, and manufacturer for all of the experimental equipment used to collect the rotational data from the magnetic single pendulum under base excitation.

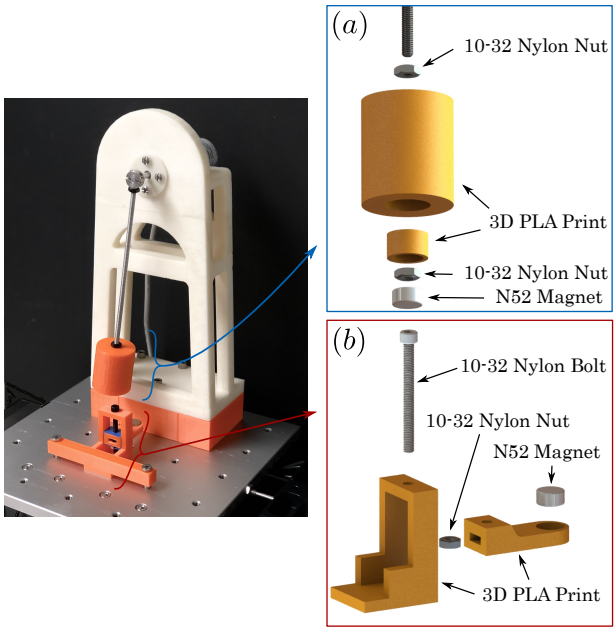

Figure 11: Manufacturing overview with experimental setup. In Fig. (a), an exploded view of the end mass (100% infill 3D printed PLA components) is shown with the magnet press fit into end of pendulum. In Fig. (b), an exploded view of the linear stage controlling the vertical position of the lower magnet.

Item	Description	Manufacturer
Shaker	113 Electro-Seis	APS
DC Power Supply	Model 1761	BK Precision
Accelerometer	Model 352C22	Piezotronics
Rotary Encoder	UCD-AC005-0413	Posital
Data Acquisition	USB-6356	Nat. Inst.
PC	OptiPlex 7050	Dell

Table 1: Equipment used for experimental data collection.

4.3 Physical Parameters and Constants

To estimate the magnetic dipole moment m of the cylindrical magnets used (see Fig. 11), a similar experiment to the one done in [1] was used. It was predicted that the magnets could not be modeled as a dipole when the distance between the magnets is less than a critical value r_c. When $r < r_c$, the dipole model should not accurately estimate the repulsive force between the magnets. This distance was estimated as $r_c = 0.035$ m (see Fig. 12). Additionally, in the region where $r > r_c$, the force curve, a function of scale r^{-4}, was fit to the curve to estimate the magnetic dipole moment as $m = 0.85$ Cm.

The other parameter values as well as their uncertainties are provided in Table 2, which are in reference to Fig. 9. Most of these parameters were either estimated using *SolidWorks* or by multiple direct measurements.

To validate the parameters, an experiment and simulation of a free drop of the pendulum are compared. The resulting angle $\theta(t)$ is shown in Fig. 13, which shows a very similar response between simulation and experiment. Additionally, the simulation is within the bounds of uncertainty of the encoder as shown in the zoomed in region of Fig. 13.

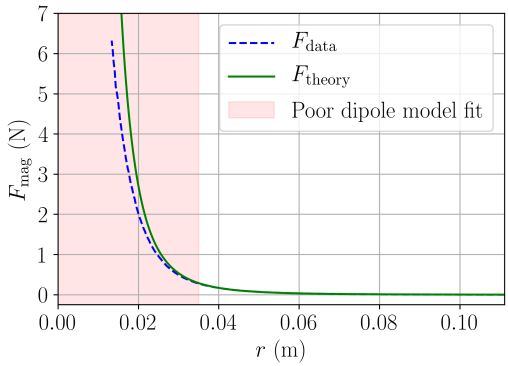

Figure 12: Collected repulsion force as a function of distance compared to theoretical force in Eq. (9) with $\theta = 0$. The theoretical force F_{theory} is based on dipole mode with a dipole moment $m = 0.85$ Cm, which was estimated using a curve fit to the region where the magnetic thickness $T << r$. Region of poor fit shown for $r < 0.035$ m.

Parameter (units)	Value	Uncertainty ($\pm\sigma$)
d (m)	0.36	0.005
ℓ (m)	0.208	0.005
g (m/s^2)	9.81	-
M (kg)	0.1038	0.005
r_{cm} (m)	0.188	-
ω (rad/s)	3π	-
μ_0 (Cm)	1.257×10^{-6}	-
m (Cm)	0.85	-
μ_c (-)	0.002540	0.000020
μ_v (-)	0.000015	0.000003
μ_q (-)	0.000151	0.000020

Table 2: Equation of motion parameters to simulated pendulum with assocaited uncertainty.

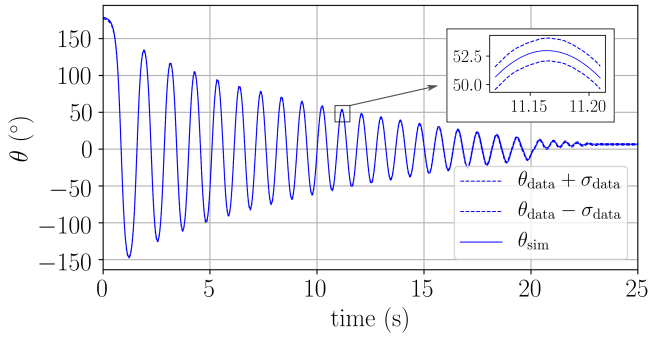

Figure 13: Free drop test between collect angular position data θ_{data} with encoder uncertainty σ_{data} and the simulated response θ_{sim}. As shown in the zoomed-in region, the simulated response is within the bounds of uncertainty of the actual response.

A Supplemental information

A.1 Bill of Materials

Table 3: Bill of Materials based on 2018 costs. This bill of materials is for the simple pendulum only (no calibration stand).

	Product	**Qty**	**Unit Cost ($)**	**Total($)**
1	IXARC MCD-AVP02-0412-R060 Absolute rotary encoder	1	382	382
2	Clamping Precision Flexible Shaft Couple	1	43.51	43.51
3	Stainless Steel Ball Bearing	1	6.38	6.38
4	0.1875 in. Precision Ground Rod	1	4.94	4.94
5	8-32 Pan Head Cap Screw 0.5 in. depth	8	0.1	0.8
6	Plastic Washer	8	0.05	0.4
7	8-32 Threaded Inasert E-Z LOK	8	1.59	12.74
8	Split Couple	1	4.5	4.5
7	10-32 Steel Threaded Rod 8.0 in. length	1	7.25	7.25
10	8-32 Hex Nut	5	0.40	1.98
11	316 Steel Washer	3	0.18	0.55
12	18-8 Steel Hex Drive Flat Head Screw	3	0.08	0.24
13	Base Magnet	3	N/A	N/A
14	Self Aligning Pad	3	N/A	N/A

A.2 Mechanical Drawings

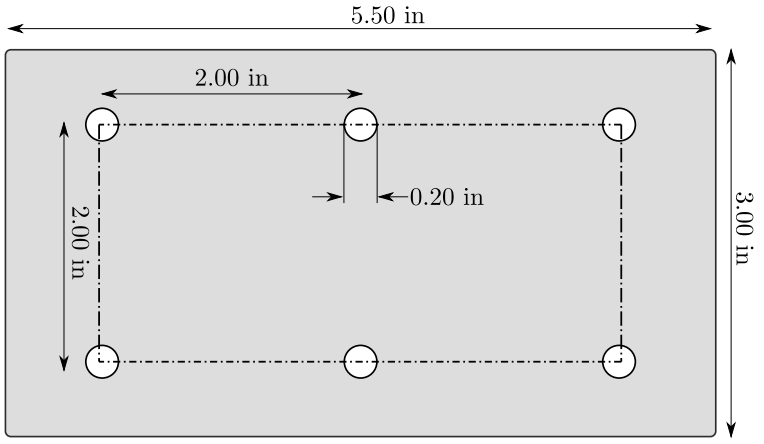

Figure 14: Hole spacing for pedestal to table screws. All dimensions are shown in inches

References

[1] Manuel I González. Forces between permanent magnets: experiments and model. *European Journal of Physics*, 38(2):025202, dec 2016.

[2] Giorgi Khomeriki. Parametric resonance induced chaos in magnetic damped driven pendulum. *Physics Letters A*, 380(31-32):2382–2385, 2016.

[3] David Petrushenko and Firas A. Khasawneh. Uncertainty propagation of system parameters to the dynamic response: An application to a benchtop pendulum. In *Volume 4B: Dynamics, Vibration, and Control*. American Society of Mechanical Engineers, nov 2017.

[4] Azad Siahmakoun, Valentina A French, and Jeffrey Patterson. Nonlinear dynamics of a sinusoidally driven pendulum in a repulsive magnetic field. *American Journal of Physics*, 65(5):393–400, 1997.

[5] Vy Tran, Eric Brost, Marty Johnston, and Jeff Jalkio. Predicting the behavior of a chaotic pendulum with a variable interaction potential. *Chaos: An Interdisciplinary Journal of Nonlinear Science*, 23(3):033103, sep 2013.